Observation of $\psi(3686) \rightarrow 3\phi$

M. Ablikim *et al.*[*]

(BESIII Collaboration)

Using $(2.712 \pm 0.014) \times 10^9$ $\psi(3686)$ events collected by the BESIII detector operating at the BEPCII collider, we report the first observation of $\psi(3686) \rightarrow 3\phi$ decay with a significance larger than 10σ. The branching fraction of this decay is determined to be $(1.46 \pm 0.05 \pm 0.17) \times 10^{-5}$, where the first uncertainty is statistical and the second is systematic. No significant structure is observed in the $\phi\phi$ invariant mass spectra.

I. INTRODUCTION

Charmonium resonances lie in between the perturbative and nonperturbative regimes of quantum chromodynamics (QCD) [1–3], which describes the strong interaction. Below the open charm threshold, both J/ψ and $\psi(3686)$ mainly decay into light hadrons through the annihilation of the $c\bar{c}$ pair into three gluons or one single virtual photon, with the decay width proportional to the modules of the charmonium wave function [4]. QCD has been tested thoroughly at high energy region where the strong interaction coupling constant is small. However, in the low energy region, theoretical calculations based on first principles of QCD are still unreliable since the nonperturbative contribution is significant, and various effective field theories are introduced [5–7] to approximate these nonperturbative contributions. The study of charmonium decays can provide valuable insights to improve the understanding of the inner charmonium structure and test phenomenological mechanisms of nonperturbative QCD.

In recent years, significant progress has been made in experimental studies of multibody J/ψ and $\psi(3686)$ decays. Previously, the $\psi(3686) \rightarrow PPP$, $\psi(3686) \rightarrow VPP$, and $\psi(3686) \rightarrow VVP$ decays have been extensively studied, as summarized in Ref. [1], where P and V denote pseudoscalar and vector mesons, respectively. To date, no study of $\psi(3686) \rightarrow VVV$ has been reported. In this paper, we present the first observation of the $\psi(3686) \rightarrow 3\phi$ decay. This analysis is based on $(2.712 \pm 0.014) \times 10^9$ $\psi(3686)$ events collected at the center-of-mass energy

of 3.686 GeV by the BESIII detector in 2009, 2012, and 2021 [8].

II. BESIII EXPERIMENT AND MONTE CARLO SIMULATION

The BESIII detector [9] records symmetric e^+e^- collisions provided by the BEPCII storage ring [10] in the center-of-mass energy ($\sqrt{s}$) range from 2.0 to 4.95 GeV, with a peak luminosity ($\mathcal{L}$) of 1×10^{33} cm^{-2} s^{-1} achieved at $\sqrt{s} = 3.77$ GeV. BESIII has collected large data samples in this energy region [1,11,12]. The cylindrical core of the BESIII detector covers 93% of the full solid angle and consists of a helium-based multilayer drift chamber, a plastic scintillator time-of-flight system (TOF), and a CsI(Tl) electromagnetic calorimeter, which are all enclosed in a superconducting solenoidal magnet providing a 1.0 T magnetic field. The solenoid is supported by an octagonal flux-return yoke with resistive plate counter muon identification modules interleaved with steel. The charged-particle momentum resolution at 1 GeV/c is 0.5%, and the dE/dx resolution is 6% for electrons from Bhabha scattering. The electromagnetic calorimeter measures photon energies with a resolution of 2.5% (5%) at 1 GeV in the barrel (end cap) region. The time resolution in the TOF barrel region is 68 ps, while that in the end cap region was 110 ps. The end cap TOF system was upgraded in 2015 using multigap resistive plate chamber technology, providing a time resolution of 60 ps, which benefits about 85% of the data used in this analysis [13].

Simulated data samples are produced with a GEANT4-based [14] Monte Carlo (MC) package, which includes the geometric description of the BESIII detector and the detector response. The simulations model the beam energy spread and initial state radiation in the e^+e^- annihilations with the generator KKMC [15]. To estimate backgrounds, an inclusive MC sample is generated including the production of the $\psi(3686)$ resonance, the initial state radiation

---

[*]Full author list given at the end of the article.

production of the J/ψ, and the continuum processes incorporated in KKMC [15]. All particle decays are modeled with EvtGen [16] using branching fractions either taken from the Particle Data Group (PDG) [17], when available, or otherwise estimated with LUNDCHARM [18]. Final state radiation from charged final state particles is incorporated using the PHOTOS package [19]. The detection efficiency of the $\psi(3686) \to 3\phi$ decay is determined using the signal MC samples containing 5×10^5 events, where the $\psi(3686) \to 3\phi$ and $\phi \to K^+K^-$ decays are generated with phase space (PHSP) and vector to scalar scalar (VSS) models, respectively. The PHSP model represents the generic PHSP for n-body decays, averaging over the spins of initial and final state particles. The VSS model describes the decay of a vector particle (ϕ) into two scalar particles.

In addition, the data sample collected at the center-of-mass energy of 3.773 GeV with an integrated luminosity of 7.93 fb^{-1} [20] is used to estimate the contribution from continuum process.

III. EVENT SELECTION

In this analysis, candidate events for $\psi(3686) \to 3\phi$ are selected by reconstructing three or two ϕ candidates. The two reconstruction methods are hereafter referred to as "full reconstruction" for the three ϕ case and "partial reconstruction" for the two ϕ case. A ϕ candidate is reconstructed by the decay $\phi \to K^+K^-$.

Each kaon candidate must satisfy $|\cos\theta| < 0.93$, where θ is the polar angle defined with respect to the z axis, which is the symmetry axis of the multilayer drift chamber. Additionally, each kaon candidate must originate within 1 cm (10 cm) of the interaction point in the plane transverse to the beam direction (in the beam direction).

Particle identification (PID) is performed on kaon candidates using the dE/dx and TOF information. The charged kaons are identified by comparing the likelihoods for the kaon and pion hypotheses and requiring $\mathcal{L}(K) > \mathcal{L}(\pi)$.

A. Full reconstruction sample

A four-constraint (4C) kinematic fit, ensuring energy and momentum conservation, is performed under the hypothesis of $e^+e^- \to 3(K^+K^-)$ with at least six good kaon candidates. The helix parameters of charged tracks in the MC simulations are corrected to improve the χ^2 distribution consistency between data and MC simulation using the method described in Ref. [21]. Events satisfying $\chi^2_{4C} < 50$ are retained for further analysis. If there are multiple combinations in an event, then the combination with the lowest χ^2_{4C} is kept for further analysis.

The three K^+K^- pairs result in six combinations to form the three different ϕ candidates. The best combination of three ϕ candidates is selected by minimizing

$$\Delta = \sqrt{\sum_{i=a,b,c} (M^i_{K^+K^-} - m_\phi)^2}, \qquad (1)$$

where m_ϕ is the nominal ϕ mass [17]. The three ϕ candidates are randomly labeled by using the Knuth-Durstenfeld shuffle algorithm [22,23], since they are identical in the reconstruction procedure.

B. Partial reconstruction sample

To improve the detection efficiency, we employ the partial reconstruction strategy when six kaon candidates cannot be reconstructed. The reconstruction of the $\psi(3686) \to 3\phi$ decay is performed by selecting exactly five kaon candidates from six charged tracks in each event, with at least two kaons of each charge. Events with less than five identified kaons are not used because of the very high combinatorial background.

The two K^+K^- pairs along with one $K^\pm$ result in six combinations to form the two ϕ candidates. The best combination of two ϕ candidates is selected by minimizing

$$\Delta = \sqrt{\sum_{i=a,b} (M^i_{K^+K^-} - m_\phi)^2 + (M^{\text{rec}}_\phi - m_\phi)^2}, \qquad (2)$$

where M^{rec}_ϕ is defined as

$$M^{\text{rec}}_\phi = \sqrt{(\sqrt{s} - E_{\phi\phi})^2 - p^2_{\phi\phi}}, \qquad (3)$$

in which $E_{\phi\phi}$ and $p_{\phi\phi}$ are the energy and momentum of the two ϕ system, respectively. Additionally, to further improve the purity of the signal sample, the recoil mass of the $2(K^+K^-)K^\pm$ combination is required to be in the mass interval of $(0.4746, 0.5145)$ GeV/c^2. This range corresponds to about $\pm 3\sigma$ around the kaon mass, where σ is the resolution on the $2(K^+K^-)K^\pm$ recoil mass. Similar to the full reconstruction case, the two reconstructed ϕ candidates are randomly labeled.

C. Background analysis

Potential background components are investigated by analyzing the inclusive MC sample of $\psi(3686)$ decays with the generic event type analysis tool, TopoAna [24]. The study shows that only a very small background contribution survives the event selection. After imposing all selection criteria, the three dimensional (3D) distributions of the invariant masses of the three ϕ candidates in the data are shown in Fig. 1 for both full and partial reconstruction cases. In both cases, a distinct cluster around the ϕ mass is evident.

IV. RESULTS

A. Fitting of data

The signal yield of the $\psi(3686) \to 3\phi$ decay is determined through a simultaneous unbinned maximum

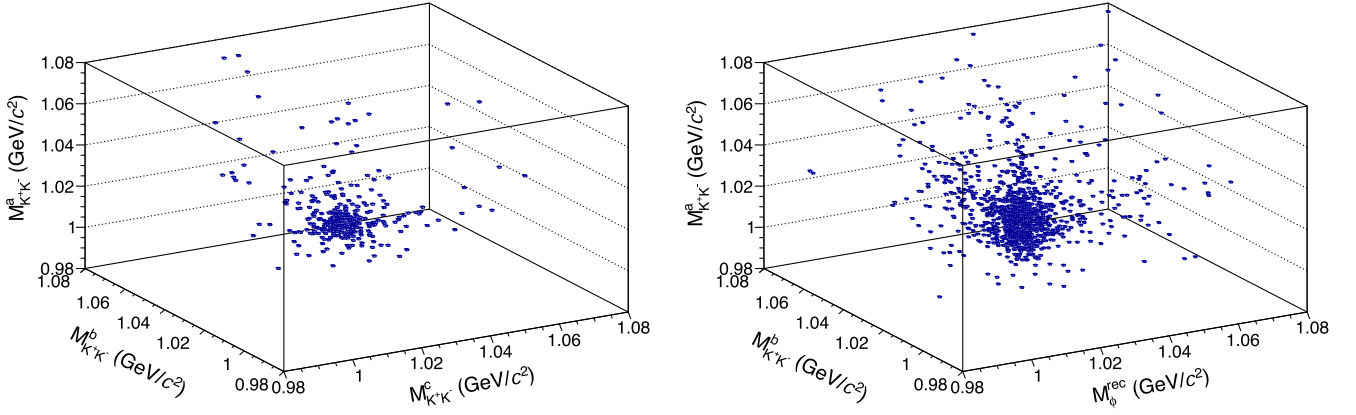FIG. 1. The $M^a_{K^+K^-} : M^b_{K^+K^-} : M^c_{K^+K^-}(M^{\mathrm{rec}}_\phi)$ distributions of the (left) full and (right) partial reconstructed candidates for $\psi(3686) \to 3\phi$.

likelihood fit to the 3D distribution of $M^a_{K^+K^-} : M^b_{K^+K^-} : M^c_{K^+K^-}$ for the full reconstruction case, and to the 3D distribution of $M^a_{K^+K^-} : M^b_{K^+K^-} : M^{\mathrm{rec}}_\phi$ for the partial reconstruction case. In the simultaneous fit, the branching fractions of $\psi(3686) \to 3\phi$ measured with the different reconstruction cases are constrained to be equal. Events are divided into four cases based on the source of the K^+K^- pairs: the "Signal" describes candidates where all three pairs of K^+K^- originate from ϕ mesons; the "BKGI" denotes candidates where two pairs of K^+K^- originate from ϕ mesons and one pair from combinatorial backgrounds; the "BKGII" describes candidates where only one pair of K^+K^- comes from the ϕ meson and the remaining two pairs are from combinatorial backgrounds; the "BKGIII" encompasses candidates where all three pairs of K^+K^- come from combinatorial backgrounds, as well as the incorrectly reconstructed events with different final states.

So, the probability density functions (PDFs) of Signal, BKGI, BKGII, and BKGIII are constructed as follows:

(1) Signal: $\mathcal{S}_x \times \mathcal{S}_y \times \mathcal{S}_z$,
(2) BKGI: $f_1 \times \mathcal{S}_x \times \mathcal{S}_y \times \mathcal{A}_z + \mathcal{S}_x \times \mathcal{A}_y \times \mathcal{S}_z + \mathcal{A}_x \times \mathcal{S}_y \times \mathcal{S}_z$,
(3) BKGII: $\mathcal{S}_x \times \mathcal{A}_y \times \mathcal{A}_z + \mathcal{A}_x \times \mathcal{S}_y \times \mathcal{A}_z + f_2 \cdot \mathcal{A}_x \times \mathcal{A}_y \times \mathcal{S}_z$,
(4) BKGIII: $\mathcal{A}_x \times \mathcal{A}_y \times \mathcal{A}_z$.

Here, x, y, and z correspond to the three dimensions of the 3D fit. The $\mathcal{S}_i$ are the signal shapes derived from signal MC simulations, while $\mathcal{A}_i$ are the reversed ARGUS functions [25] that characterize the combinatorial background shape in the K^+K^- invariant mass spectrum, where i denotes the different dimensions. The parameters f_1 and f_2 describe the distinct PDFs resulting from the nonidentical ϕ reconstructions in the partial reconstruction sample. This disparity is attributed to the resolution differences between the full and partial reconstructions. While f_1 and f_2 are fixed to 1 for the full reconstruction sample, they are treated as free fit parameters for the partial reconstruction sample to incorporate the resolution variation.

For the full reconstruction case, the $\mathcal{S}_i$ are identical and determined from the ϕ candidates of signal MC simulations. Additionally, $\mathcal{A}_i$ are identical reversed ARGUS functions with starting points fixed at the K^+K^- mass threshold.

For the partial reconstruction case, we specify the z as the recoil dimension. $\mathcal{S}_x$ and $\mathcal{S}_y$ are identical PDFs derived from the two fully reconstructed ϕ candidates and $\mathcal{S}_z$ is derived from the line shape of M^{rec}_ϕ of signal MC simulations. $\mathcal{A}_x$ and $\mathcal{A}_y$ share the same parameters, while the parameters of $\mathcal{A}_z$ are independently determined. The starting points of all $\mathcal{A}_i$ are fixed at the K^+K^- mass threshold.

B. Detection efficiency

The detection efficiency of the $\psi(3686) \to 3\phi$ decay is evaluated by analyzing the signal MC samples. Figure 2 shows the Dalitz plots of the $\psi(3686) \to 3\phi$ candidates selected in data and signal MC samples. Figures 3 and 4 show the comparisons of the momenta and cosines of polar angles of each ϕ candidate, as well as the K^+K^- invariant mass spectra between data and MC simulation. The consistency between data and MC simulation is good. The detection efficiencies of $\psi(3686) \to 3\phi$ is determined to be $(6.13 \pm 0.04)\%$ and $(20.58 \pm 0.08)\%$ for full and partial reconstruction samples, respectively. An efficiency correction factor is applied to account for the data-MC deviation arising from tracking and PID efficiencies for $K^\pm$, as listed in Sec. V.

C. Branching fraction

Under the assumption that there is no interference between the $\psi(3686)$ and continuum amplitudes, the branching fraction of the $\psi(3686) \to 3\phi$ decay is determined as follows:

$$\mathcal{B}_{\psi(3686)\to3\phi} = \frac{N_{(3686)\to3\phi} - f_c \times N_{(3773)\to3\phi}}{N_{\psi(3686)}\mathcal{B}^3_{\phi\to K^+K^-}\epsilon_{\psi(3686)\to3\phi}}, \quad (4)$$
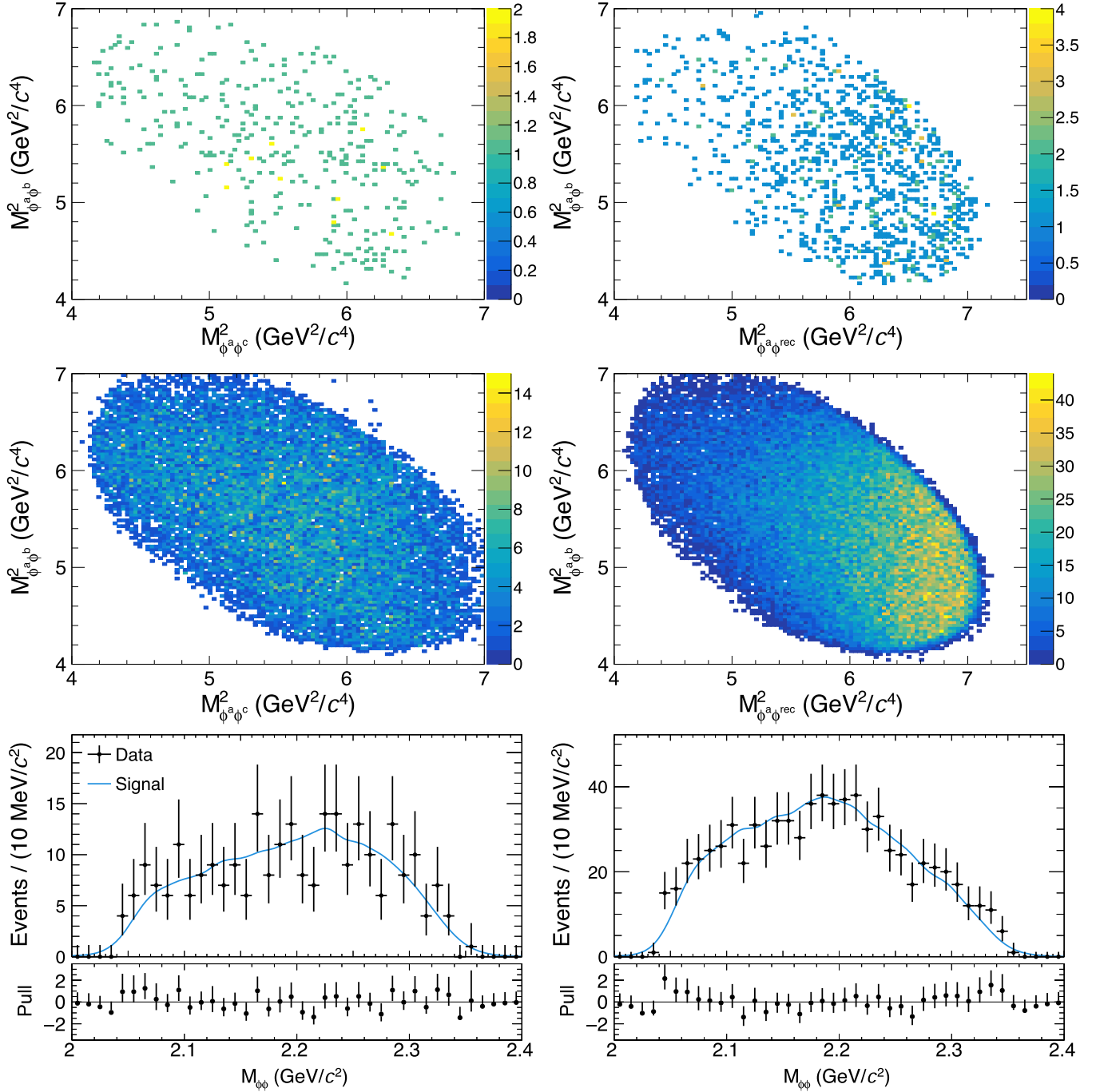
FIG. 2.   Dalitz plots of $M^2_{\phi^a\phi^b}$ vs $M^2_{\phi^a\phi^c}$ of the (left) full and (right) partial reconstructed candidates. The first row indicates data and the second row indicates signal MC events. In the third row, the distributions of the invariant masses of the two lowest momentum ϕ candidates are shown. The black points with error bars are data. The blue curves represent the signal component of the fit.

where $N_{(3686)\to3\phi}$ and $N_{(3773)\to3\phi}$ are the observed numbers of 3ϕ candidates extracted from the data sample taken at $\sqrt{s} = 3.686$ and 3.773 GeV. They are determined to be 1319 ± 43 and 138 ± 15, also the fractions of full reconstructed events out of total events are 23% and 27%. Figures 5 and 6 show the fit results on the selected candidates. Meanwhile the fitted event numbers of BKGI, BKGII, and BKGIII are 74 ± 24, 30 ± 16, and 48 ± 16.

The factor f_c is introduced to propagate the number of continuum events observed at 3.773 GeV to the 3.686 GeV energy point taking into account luminosities [8] $\mathcal{L}_{3.686(3.773)}$ and cross sections at different energies. It is calculated as $f_c = \frac{\epsilon_{\psi(3686)\to3\phi}}{\epsilon_{e^+e^-(3773)\to3\phi}} \times \frac{\mathcal{L}_{3.686}}{\mathcal{L}_{3.773}} \times \frac{(3.773 \text{ GeV})^{2n}}{(3.686 \text{ GeV})^{2n}}$, where n is the power of the $\frac{1}{s}$ dependence of the cross section. We take $n = 1$ [26] and obtain $f_c = 0.49$. The total number of
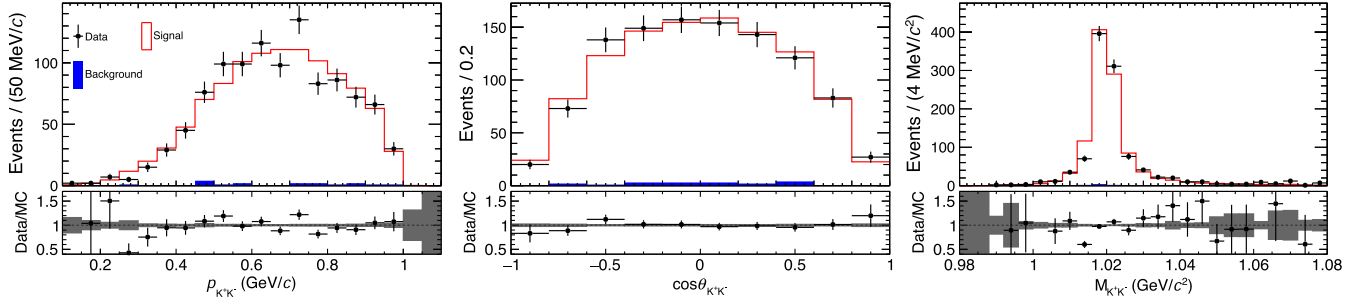
FIG. 3. Distributions of the momentum, cosines of polar angle and mass spectra of the ϕ candidates for full reconstructed candidates, all reconstructed ϕ candidates are filled in the same histogram. The black points with error bars are data, the solid red lines show the signal MC simulation which is scaled to the total number of events of data, and the blue solid-filled histograms are the background contribution of the inclusive MC sample. The bottom panels show the data and MC comparison, where the error bands indicate the MC statistical uncertainty only.

$\psi(3686)$ events is labeled as $N_{\psi(3686)}$ and $\mathcal{B}_{\phi \to K^+ K^-}$ is the world average value of the branching fraction of $\phi \to K^+ K^-$ taken from the PDG [17]. The detection efficiencies for $\psi(3686) \to 3\phi$ and the continuum process $e^+ e^- (3773) \to 3\phi$ are labeled as $\epsilon_{\psi(3686) \to 3\phi}$ and $\epsilon_{e^+ e^- (3773) \to 3\phi}$. The branching fraction of the $\psi(3686) \to 3\phi$ decay is determined to be $(1.46 \pm 0.05) \times 10^{-5}$, where the uncertainty is statistical only.

The statistical significance is estimated by examining the probability of the change in negative log-likelihood values when the signal is included or excluded in the fits. This probability is calculated under the χ^2 distribution hypothesis taking into account the change in the number of degrees of freedom. Consequently, the significance is determined to be greater than 10σ.

We have also examined the Dalitz plot and $\phi\phi$ invariant mass spectra, as shown in Fig. 2, and no obvious structure is found.

V. SYSTEMATIC UNCERTAINTIES

The systematic uncertainties in the measurement of the branching fraction of the $\psi(3686) \to 3\phi$ are discussed below.

The total number of $\psi(3686)$ events has been determined to be $N_{\psi(3686)} = (2.712 \pm 0.014) \times 10^9$ with inclusive hadronic events as described in Ref. [8]. This measurement contributes 0.5% to the systematic uncertainty of the branching fraction.

The systematic uncertainties of $K^\pm$ tracking and PID are studied with the control sample of $e^+ e^- \to \pi^+ \pi^- J/\psi$ ($J/\psi \to K^+ K^- K^+ K^-$). The differences of $K^\pm$ tracking and PID efficiencies between data and MC simulation are obtained in different transverse momentum intervals. The data-MC differences are then weighted according to the distribution of the transverse momentum of kaon in the signal decay. The data to MC ratios of the reweighted tracking and PID efficiencies are $(98.86 \pm 0.55)\%$ and $(99.50 \pm 0.05)\%$, respectively. Here the errors

originate mainly from the limited statistics of the control sample. The detection efficiency estimated from the MC is corrected with the data to MC ratios, and the rounded uncertainties of the ratios, 0.6% and 0.1%, are taken as the systematic uncertainty of the tracking and PID efficiencies per $K^\pm$, respectively.

The systematic uncertainty of the 3D fit is considered in three aspects. The background shape is changed from the reversed ARGUS function to a second-order polynominal function. The signal shape is changed from the simulated MC shape to the shape used by *BABAR* [27], written as

$$\sigma(s) = \frac{1}{s^{5/2}} \frac{q_{K^+ K^-}^3(s)}{q_{K^+ K^-}^3(m_\phi^2)} \left| \frac{\Gamma_\phi m_\phi^3 \sqrt{m_\phi \sigma_{\phi \to K^+ K^-}/C}}{s - m_\phi^2 + i\sqrt{s}\Gamma_\phi \frac{q_{K^+ K^-}^3(s)}{q_{K^+ K^-}^3(m_\phi^2)}} \right|^2, \quad (5)$$

where $q_{K^+ K^-}(s) = \sqrt{s - 4m_{K^\pm}^2}$ is a threshold term; $\sigma_{\phi \to K^+ K^-}$ is a normalization factor obtained from the fit; $C = 0.389 \times 10^{12}$ nb MeV$^2/c^4$; m_ϕ and Γ_ϕ are the mass and width of the ϕ meson. The alternative fit ranges are chosen as [0.98, 1.09], [0.98, 1.07], [0.97, 1.08], and [0.99, 1.08] GeV/c^2. The quadratic sum of the signal yield variations, 5.7%, is assigned as the corresponding systematic uncertainty.

The effect of the misidentification of the potential backgrounds from $\psi(3686) \to 2\phi K^+ K^-$, $\psi(3686) \to \phi 2(K^+ K^-)$, and $\psi(3686) \to 3(K^+ K^-)$ to signal are found to be less than 0.1% and are thereby ignored in the systematic uncertainty.

In the nominal analysis, the helix parameters of charged tracks in the 4C kinematic fit have been corrected with the parameters derived with the control sample of $e^+ e^- \to K^*(892) K \pi \to K K \pi \pi$ in Ref. [21]. The difference of detection efficiencies with and without helix parameter correction, 1.7%, is assigned as the corresponding systematic uncertainty.

In the nominal analysis, the M_{rec}^K is required to be within the $\pm 3\sigma$ interval around the kaon mass. Changing this
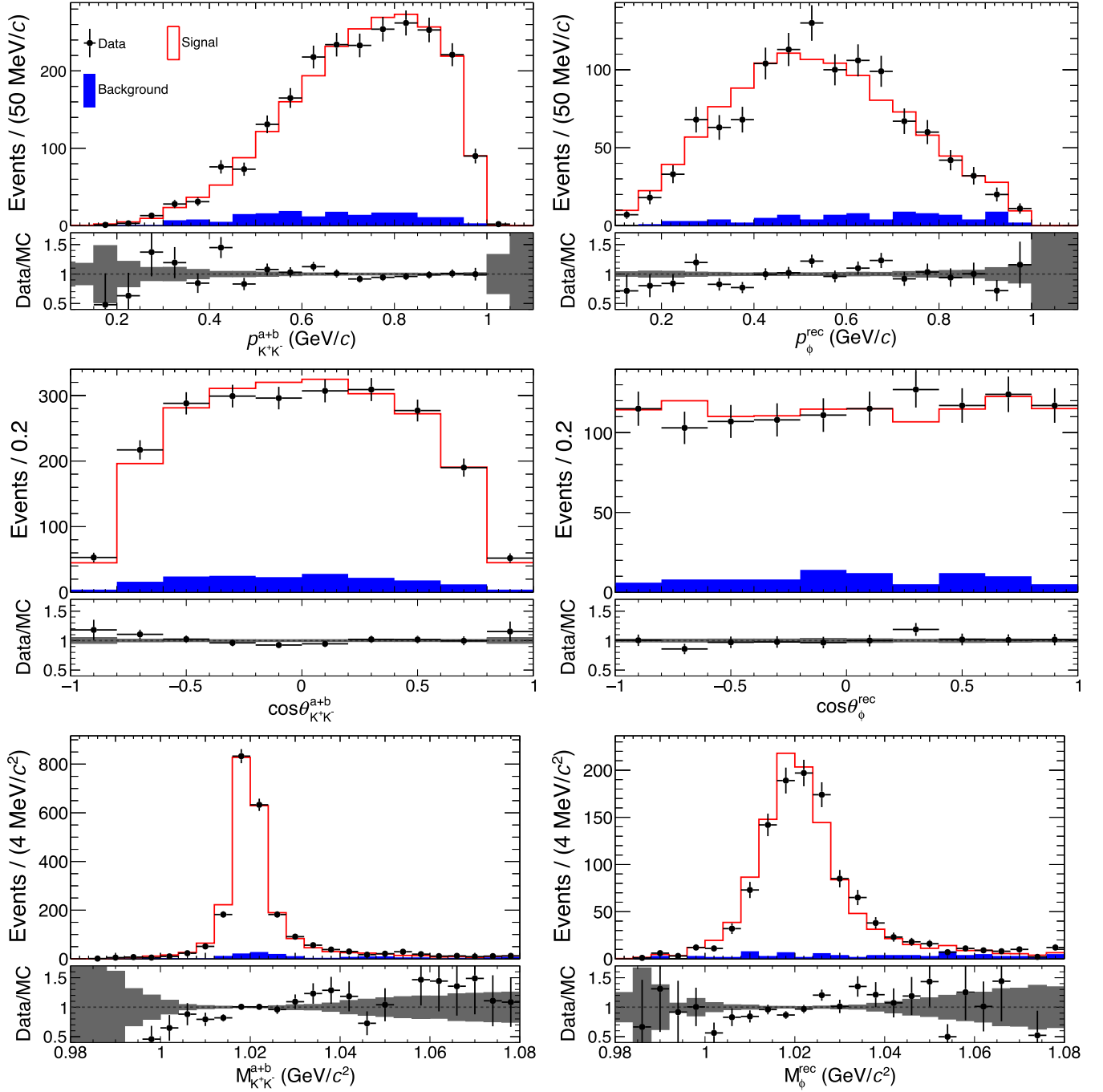
FIG. 4. Distributions of the momentum, cosines of polar angle and mass spectra of the ϕ candidates for partial candidates, two reconstructed ϕ candidates are filled in the same histogram (first column). The black points with error bars are data, the solid red lines show the signal MC simulation which is scaled to the total number of events of data, and the blue solid-filled histograms are the background contribution of the inclusive MC sample. The bottom panels show the data and MC comparison, where the error bands indicate the MC statistical uncertainty only.

interval to $\pm 2\sigma$ or $\pm 4\sigma$ results in a relative change of the measured signal by 1.0%, which is taken as a systematic uncertainty.

Another source of the systematic uncertainty is the limited MC statistics. This contribution is evaluated as

$$\frac{1}{\sqrt{N}}\sqrt{\frac{(1-\epsilon)}{\epsilon}}, \tag{6}$$
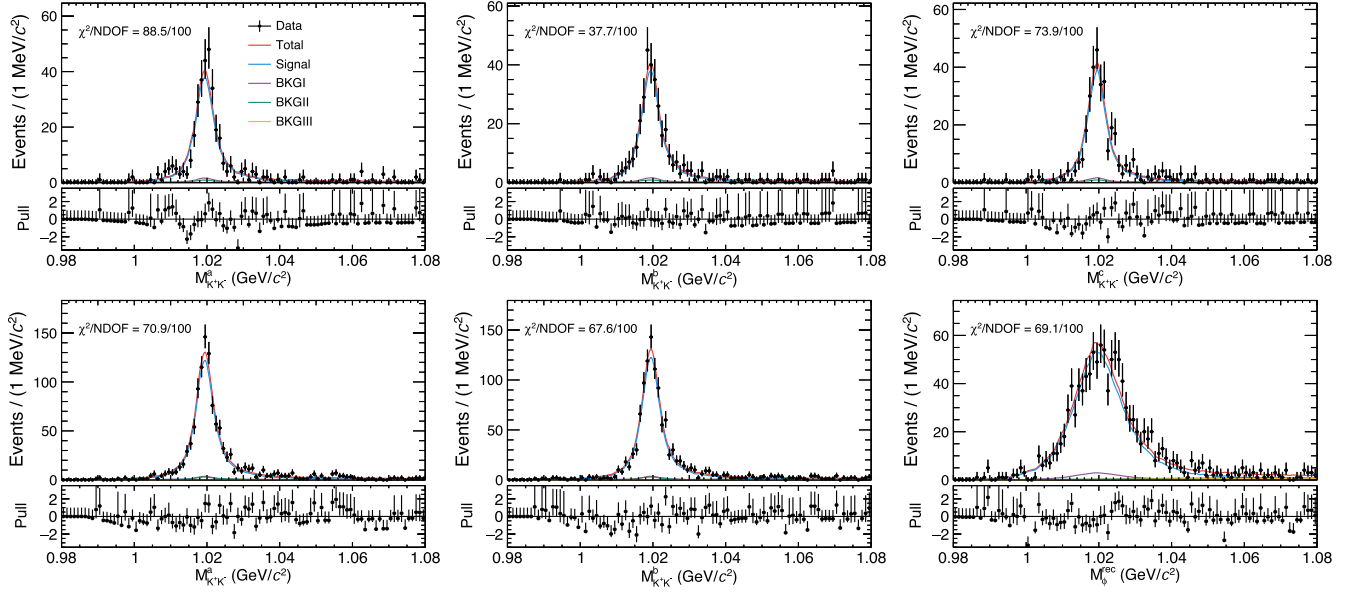
FIG. 5. One-dimensional projections of the simultaneous fit to the $M_{K^+K^-}^a$: $M_{K^+K^-}^b$: $M_{K^+K^-}^c$ (M_ϕ^{rec}) distribution of the (top row) full and (bottom row) partial reconstructed candidate events of $\psi(3686) \to 3\phi$ for $\psi(3686)$ data (shown as the dots with error bars). The red solid curves are the total fit results, while the blue curves are the signal contributions of the fit and other curves represent the different background contributions. For each projection, the χ^2/NDOF are provided, with χ^2 being calculated from the difference between the binned data points and the total fit projection, and the NDOF representing the number of bins.
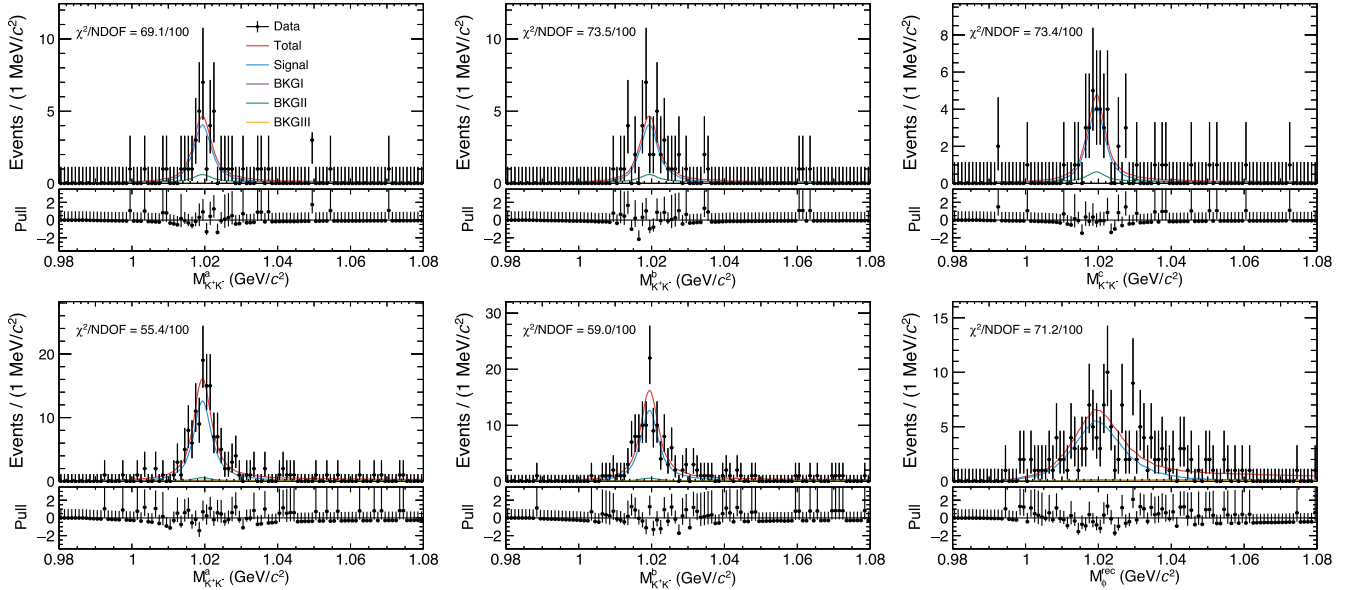
FIG. 6. One-dimensional projections of the simultaneous fit to the $M_{K^+K^-}^a$: $M_{K^+K^-}^b$: $M_{K^+K^-}^c$ (M_ϕ^{rec}) distribution of the (top row) full and (bottom row) partial reconstructed candidate events of $e^+e^- \to 3\phi$ for data taken at 3.773 GeV (shown as the dots with error bars). The red solid curves are the total fit results, while the blue curves are the signal contributions of the fit and other curves represent the different background contributions. For each projection, the χ^2/NDOF are given, with χ^2 being calculated from the difference between the binned data points and the total fit projection, and the NDOF representing the number of bins.

where ϵ is the detection efficiency and N is total number of signal MC events. The corresponding number, 0.4%, is assigned as the systematic uncertainty.

The branching fraction $(49.1 \pm 0.5)\%$ of $\phi \to K^+K^-$ is quoted from the PDG [17], contributing a relative uncertainty of 1.0%.

In the nominal analysis, we determine the branching fraction without considering the interference between $\psi(3686)$ and continuum amplitudes. The systematic uncertainty due to this effect is estimated by introducing an interference term between psi(3686) and continuum amplitudes. The largest relative change of the signal yield, 9.0%,

TABLE I. Systematic uncertainties in the branching fraction measurement.

Source	Full (%)	Partial (%)
$N_{\psi(3686)}$	0.5	0.5
Tracking	3.6	3.0
PID	0.6	0.5
3D fit	5.7	5.7
4C kinematic fit	1.7	None
M_{rec}^K requirement	None	1.0
MC statistics	0.4	0.4
$\mathcal{B}(\phi \to K^+ K^-)$	3.0	3.0
Interference	9.0	9.0
Total	11.8	11.5

which is observed for $\pm 90°$ phase between the two amplitudes, is taken as the systematic error.

All the systematic uncertainties are summarized in Table I. The total uncertainty for each reconstruction case in the Table I is calculated as a quadratic sum of all contributions, which are assumed to be independent within each case. The total systematic uncertainty is calculated using the method described in [28], which takes into account the correlations of systematic uncertainties between the different reconstruction cases. The uncertainties from the 4C kinematic fit, the M_{rec}^K requirement, and MC statistics are taken as uncorrelated and all other contributions are assumed to be fully correlated between the two reconstruction cases. The total systematic uncertainty is determined to be 11.5%.

VI. SUMMARY

By analyzing $(2.712 \pm 0.014) \times 10^9$ events collected with the BESIII detector operating at the BEPCII collider, we report the first observation of the $\psi(3686) \to 3\phi$ decay. The branching fraction of this decay is determined to be $(1.46 \pm 0.05 \pm 0.17) \times 10^{-5}$, with the first uncertainty being statistical and the second one systematic. Furthermore, we have examined the Dalitz plots and found no obvious structure. Further studies with high statistics data taken at the future super tau-charm factory [29] will be valuable to deeply understand the decay mechanisms of these types of decays and to seek potential new structures in the $\phi\phi$ mass spectrum.

[1] M. Ablikim *et al.* (BESIII Collaboration), Chin. Phys. C **44**, 040001 (2020).

[2] W. Kwong, J. L. Rosner, and C. Quigg, Annu. Rev. Nucl. Part. Sci. **37**, 325 (1987).

[3] E. Eichten, S. Godfrey, H. Mahlke, and J. L. Rosner, Rev. Mod. Phys. **80**, 1161 (2008).

[4] T. Appelquist and H. D. Politzer, Phys. Rev. Lett. **34**, 43 (1975); A. De Rujula and S. L. Glashow, Phys. Rev. Lett. **34**, 46 (1975).

[5] E. Eichten and K. Gottfried, Phys. Lett. **66B**, 286 (1977).

[6] J. M. Drouffe and J. B. Zuber, Phys. Rep. **102**, 1 (1983).

[7] V. L. Chernyak and A. R. Zhitnitsky, Phys. Rep. **112**, 173 (1984).

[8] M. Ablikim *et al.* (BESIII Collaboration), Chin. Phys. C **42**, 023001 (2018). With the same method, the total number of $\psi(3686)$ events collected in 2009, 2012, and 2021 is determined to be $(2.712 \pm 0.014) \times 10^9$ with an uncertainty of 0.5% as a preliminary result.

[9] M. Ablikim *et al.* (BESIII Collaboration), Nucl. Instrum. Methods Phys. Res., Sect. A **614**, 345 (2010); Chin. Phys. C **44**, 040001 (2020).

[10] C. H. Yu *et al.*, in *Proceedings of IPAC 2016, Busan, Korea* (2016), ISBN 978-3-95450-147-2.

[11] J. Lu, Y. Xiao, and X. Ji, Radiat. Detect. Technol. Methods **4**, 337 (2020).

[12] J. W. Zhang, L. H. Wu, S. S. Sun *et al.*, Radiat. Detect. Technol. Methods **6**, 289 (2022).

[13] X. Li *et al.*, Radiat. Detect. Technol. Methods **1**, 13 (2017); Y. X. Guo *et al.*, Radiat. Detect. Technol. Methods **1**, 15 (2017); P. Cao *et al.*, Nucl. Instrum. Methods Phys. Res., Sect. A **953**, 163053 (2020).

[14] S. Agostinelli *et al.* (GEANT4 Collaboration), Nucl. Instrum. Methods Phys. Res., Sect. A **506**, 250 (2003).

[15] S. Jadach, B. F. L. Ward, and Z. Was, Phys. Rev. D **63**, 113009 (2001); Comput. Phys. Commun. **130**, 260 (2000).

[16] D. J. Lange, Nucl. Instrum. Methods Phys. Res., Sect. A **462**, 152 (2001); R. G. Ping, Chin. Phys. C **32**, 599 (2008).

[17] R. L. Workman *et al.* (Particle Data Group), Prog. Theor. Exp. Phys. **2022**, 083C01 (2022).

[18] J. C. Chen, G. S. Huang, X. R. Qi, D. H. Zhang, and Y. S. Zhu, Phys. Rev. D **62**, 034003 (2000); R. L. Yang, R. G. Ping, and H. Chen, Chin. Phys. Lett. **31**, 061301 (2014).

[19] E. Richter-Was, Phys. Lett. B **303**, 163 (1993).

[20] M. Ablikim *et al.* (BESIII Collaboration), Chin. Phys. C **37**, 123001 (2013); Phys. Lett. B **753**, 629 (2016). With the same method, the total luminosity of $\psi(3773)$ data sample collected in 2009, 2010, and 2022 is determined to be 7.93 fb^{-1} as a preliminary result.

[21] M. Ablikim *et al.* (BESIII Collaboration), Phys. Rev. D **87**, 012002 (2013).

[22] R. Durstenfield, Commun. ACM **7**, 420 (1964),

[23] D. E. Knuth, *Seminumerical Algorithms. The Art of Computer Programming, Vol. 2* (Addison-Wesley, Reading, MA, 1969), pp. 139-140.

[24] X. Y. Zhou, S. X. Du, G. Li, and C. P. Shen, Comput. Phys. Commun. **258**, 107540 (2021).

[25] H. Albrecht *et al.* (ARGUS Collaboration), Phys. Lett. B **241**, 278 (1990).

[26] M. Ablikim *et al.* (BESIII Collaboration), Phys. Rev. D **108**, 052001 (2023).

[27] J. P. Lees *et al.* (*BABAR* Collaboration), Phys. Rev. D **89**, 092002 (2014).

[28] Michael Schmelling, Phys. Scr. **51**, 676 (1995).

[29] M. Achasov *et al.*, Front. Phys. (Beijing)**19**, 14701 (2024).

M. Ablikim,[1] M. N. Achasov,[4,c] P. Adlarson,[75] O. Afedulidis,[3] X. C. Ai,[80] R. Aliberti,[35] A. Amoroso,[74a,74c] Q. An,[71,58,a] Y. Bai,[57] O. Bakina,[36] I. Balossino,[29a] Y. Ban,[46,h] H.-R. Bao,[63] V. Batozskaya,[1,44] K. Begzsuren,[32] N. Berger,[35] M. Berlowski,[44] M. Bertani,[28a] D. Bettoni,[29a] F. Bianchi,[74a,74c] E. Bianco,[74a,74c] A. Bortone,[74a,74c] I. Boyko,[36] R. A. Briere,[5] A. Brueggemann,[68] H. Cai,[76] X. Cai,[1,58] A. Calcaterra,[28a] G. F. Cao,[1,63] N. Cao,[1,63] S. A. Cetin,[62a] J. F. Chang,[1,58] G. R. Che,[43] G. Chelkov,[36,b] C. Chen,[43] C. H. Chen,[9] Chao Chen,[55] G. Chen,[1] H. S. Chen,[1,63] H. Y. Chen,[20] M. L. Chen,[1,58,63] S. J. Chen,[42] S. L. Chen,[45] S. M. Chen,[61] T. Chen,[1,63] X. R. Chen,[31,63] X. T. Chen,[1,63] Y. B. Chen,[1,58] Y. Q. Chen,[34] Z. J. Chen,[25,i] Z. Y. Chen,[1,63] S. K. Choi,[10] G. Cibinetto,[29a] F. Cossio,[74c] J. J. Cui,[50] H. L. Dai,[1,58] J. P. Dai,[78] A. Dbeyssi,[18] R. E. de Boer,[3] D. Dedovich,[36] C. Q. Deng,[72] Z. Y. Deng,[1] A. Denig,[35] I. Denysenko,[36] M. Destefanis,[74a,74c] F. De Mori,[74a,74c] B. Ding,[66,1] X. X. Ding,[46,h] Y. Ding,[34] Y. Ding,[40] J. Dong,[1,58] L. Y. Dong,[1,63] M. Y. Dong,[1,58,63] X. Dong,[76] M. C. Du,[1] S. X. Du,[80] Y. Y. Duan,[55] Z. H. Duan,[42] P. Egorov,[36,b] Y. H. Fan,[45] J. Fang,[1,58] J. Fang,[59] S. S. Fang,[1,63] W. X. Fang,[1] Y. Fang,[1] Y. Q. Fang,[1,58] R. Farinelli,[29a] L. Fava,[74b,74c] F. Feldbauer,[3] G. Felici,[28a] C. Q. Feng,[71,58] J. H. Feng,[59] Y. T. Feng,[71,58] M. Fritsch,[3] C. D. Fu,[1] J. L. Fu,[63] Y. W. Fu,[1,63] H. Gao,[63] X. B. Gao,[41] Y. N. Gao,[46,h] Yang Gao,[71,58] S. Garbolino,[74c] I. Garzia,[29a,29b] L. Ge,[80] P. T. Ge,[76] Z. W. Ge,[42] C. Geng,[59] E. M. Gersabeck,[67] A. Gilman,[69] K. Goetzen,[13] L. Gong,[40] W. X. Gong,[1,58] W. Gradl,[35] S. Gramigna,[29a,29b] M. Greco,[74a,74c] M. H. Gu,[1,58] Y. T. Gu,[15] C. Y. Guan,[1,63] A. Q. Guo,[31,63] L. B. Guo,[41] M. J. Guo,[50] R. P. Guo,[49] Y. P. Guo,[12,g] A. Guskov,[36,b] J. Gutierrez,[27] K. L. Han,[63] T. T. Han,[1] F. Hanisch,[3] X. Q. Hao,[19] F. A. Harris,[65] K. K. He,[55] K. L. He,[1,63] F. H. Heinsius,[3] C. H. Heinz,[35] Y. K. Heng,[1,58,63] C. Herold,[60] T. Holtmann,[3] P. C. Hong,[34] G. Y. Hou,[1,63] X. T. Hou,[1,63] Y. R. Hou,[63] Z. L. Hou,[1] B. Y. Hu,[59] H. M. Hu,[1,63] J. F. Hu,[56,j] S. L. Hu,[12,g] T. Hu,[1,58,63] Y. Hu,[1] G. S. Huang,[71,58] K. X. Huang,[59] L. Q. Huang,[31,63] X. T. Huang,[50] Y. P. Huang,[1] Y. S. Huang,[59] T. Hussain,[73] F. Hölzken,[3] N. Hüsken,[35] N. in der Wiesche,[68] J. Jackson,[27] S. Janchiv,[32] J. H. Jeong,[10] Q. Ji,[1] Q. P. Ji,[19] W. Ji,[1,63] X. B. Ji,[1,63] X. L. Ji,[1,58] Y. Y. Ji,[50] X. Q. Jia,[50] Z. K. Jia,[71,58] D. Jiang,[1,63] H. B. Jiang,[76] P. C. Jiang,[46,h] S. S. Jiang,[39] T. J. Jiang,[16] X. S. Jiang,[1,58,63] Y. Jiang,[63] J. B. Jiao,[50] J. K. Jiao,[34] Z. Jiao,[23] S. Jin,[42] Y. Jin,[66] M. Q. Jing,[1,63] X. M. Jing,[63] T. Johansson,[75] S. Kabana,[33] N. Kalantar-Nayestanaki,[64] X. L. Kang,[9] X. S. Kang,[40] M. Kavatsyuk,[64] B. C. Ke,[80] V. Khachatryan,[27] A. Khoukaz,[68] R. Kiuchi,[1] O. B. Kolcu,[62a] B. Kopf,[3] M. Kuessner,[3] X. Kui,[1,63] N. Kumar,[26] A. Kupsc,[44,75] W. Kühn,[37] J. J. Lane,[67] P. Larin,[18] L. Lavezzi,[74a,74c] T. T. Lei,[71,58] Z. H. Lei,[71,58] M. Lellmann,[35] T. Lenz,[35]

C. Li,[47] C. Li,[43] C. H. Li,[39] Cheng Li,[71,58] D. M. Li,[80] F. Li,[1,58] G. Li,[1] H. B. Li,[1,63] H. J. Li,[19] H. N. Li,[56,j] Hui Li,[43] J. R. Li,[61] J. S. Li,[59] K. Li,[1] L. J. Li,[1,63] L. K. Li,[1] Lei Li,[48] M. H. Li,[43] P. R. Li,[38,k,l] Q. M. Li,[1,63] Q. X. Li,[50] R. Li,[17,31] S. X. Li,[12] T. Li,[50] W. D. Li,[1,63] W. G. Li,[1,a] X. Li,[1,63] X. H. Li,[71,58] X. L. Li,[50] X. Y. Li,[1,63] X. Z. Li,[59] Y. G. Li,[46,h] Z. J. Li,[59] Z. Y. Li,[78] C. Liang,[42] H. Liang,[1,63] H. Liang,[71,58] Y. F. Liang,[54] Y. T. Liang,[31,63] G. R. Liao,[14] L. Z. Liao,[50] Y. P. Liao,[1,63] J. Libby,[26] A. Limphirat,[60] C. C. Lin,[55] D. X. Lin,[31,63] T. Lin,[1] B. J. Liu,[1] B. X. Liu,[76] C. Liu,[34] C. X. Liu,[1] F. Liu,[1] F. H. Liu,[53] Feng Liu,[6] G. M. Liu,[56,j] H. Liu,[38,k,l] H. B. Liu,[15] H. H. Liu,[1] H. M. Liu,[1,63] Huihui Liu,[21] J. B. Liu,[71,58] J. Y. Liu,[1,63] K. Liu,[38,k,l] K. Y. Liu,[40] Ke Liu,[22] L. Liu,[71,58] L. C. Liu,[43] Lu Liu,[43] M. H. Liu,[12,g] P. L. Liu,[1] Q. Liu,[63] S. B. Liu,[71,58] T. Liu,[12,g] W. K. Liu,[43] W. M. Liu,[71,58] X. Liu,[38,k,l] X. Liu,[39] Y. Liu,[80] Y. Liu,[38,k,l] Y. B. Liu,[43] Z. A. Liu,[1,58,63] Z. D. Liu,[9] Z. Q. Liu,[50] X. C. Lou,[1,58,63] F. X. Lu,[59] H. J. Lu,[23] J. G. Lu,[1,58] X. L. Lu,[1] Y. Lu,[7] Y. P. Lu,[1,58] Z. H. Lu,[1,63] C. L. Luo,[41] J. R. Luo,[59] M. X. Luo,[79] T. Luo,[12,g] X. L. Luo,[1,58] X. R. Lyu,[63] Y. F. Lyu,[43] F. C. Ma,[40] H. Ma,[78] H. L. Ma,[1] J. L. Ma,[1,63] L. L. Ma,[50] M. M. Ma,[1,63] Q. M. Ma,[1] R. Q. Ma,[1,63] T. Ma,[71,58] X. T. Ma,[1,63] X. Y. Ma,[1,58] Y. Ma,[46,h] Y. M. Ma,[31] F. E. Maas,[18] M. Maggiora,[74a,74c] S. Malde,[69] Y. J. Mao,[46,h] Z. P. Mao,[1] S. Marcello,[74a,74c] Z. X. Meng,[66] J. G. Messchendorp,[13,64] G. Mezzadri,[29a] H. Miao,[1,63] T. J. Min,[42] R. E. Mitchell,[27] X. H. Mo,[1,58,63] B. Moses,[27] N. Yu. Muchnoi,[4,c] J. Muskalla,[35] Y. Nefedov,[36] F. Nerling,[18,e] L. S. Nie,[20] I. B. Nikolaev,[4,c] Z. Ning,[1,58] S. Nisar,[11,m] Q. L. Niu,[38,k,l] W. D. Niu,[55] Y. Niu,[50] S. L. Olsen,[63] Q. Ouyang,[1,58,63] S. Pacetti,[28b,28c] X. Pan,[55] Y. Pan,[57] A. Pathak,[34] P. Patteri,[28a] Y. P. Pei,[71,58] M. Pelizaeus,[3] H. P. Peng,[71,58] Y. Y. Peng,[38,k,l] K. Peters,[13,e] J. L. Ping,[41] R. G. Ping,[1,63] S. Plura,[35] V. Prasad,[33] F. Z. Qi,[1] H. Qi,[71,58] H. R. Qi,[61] M. Qi,[42] T. Y. Qi,[12,g] S. Qian,[1,58] W. B. Qian,[63] C. F. Qiao,[63] X. K. Qiao,[80] J. J. Qin,[72] L. Q. Qin,[14] L. Y. Qin,[71,58] X. S. Qin,[50] Z. H. Qin,[1,58] J. F. Qiu,[1] Z. H. Qu,[72] C. F. Redmer,[35] K. J. Ren,[39] A. Rivetti,[74c] M. Rolo,[74c] G. Rong,[1,63] Ch. Rosner,[18] S. N. Ruan,[43] N. Salone,[44] A. Sarantsev,[36,d] Y. Schelhaas,[35] K. Schoenning,[75] M. Scodeggio,[29a] K. Y. Shan,[12,g] W. Shan,[24] X. Y. Shan,[71,58] Z. J. Shang,[38,k,l] L. G. Shao,[1,63] M. Shao,[71,58] C. P. Shen,[12,g] H. F. Shen,[1,8] W. H. Shen,[63] X. Y. Shen,[1,63] B. A. Shi,[63] H. Shi,[71,58] H. C. Shi,[71,58] J. L. Shi,[12,g] J. Y. Shi,[1] Q. Q. Shi,[55] S. Y. Shi,[72] X. Shi,[1,58] J. J. Song,[19] T. Z. Song,[59] W. M. Song,[34,1] Y. J. Song,[12,g] Y. X. Song,[46,h,n] S. Sosio,[74a,74c] S. Spataro,[74a,74c] F. Stieler,[35] Y. J. Su,[63] G. B. Sun,[76] G. X. Sun,[1] H. Sun,[63] H. K. Sun,[1] J. F. Sun,[19] K. Sun,[61] L. Sun,[76] S. S. Sun,[1,63] T. Sun,[51,f] W. Y. Sun,[34] Y. Sun,[9] Y. J. Sun,[71,58] Y. Z. Sun,[1] Z. Q. Sun,[1,63] Z. T. Sun,[50] C. J. Tang,[54] G. Y. Tang,[1] J. Tang,[59] M. Tang,[71,58] Y. A. Tang,[76] L. Y. Tao,[72] Q. T. Tao,[25,i] M. Tat,[69] J. X. Teng,[71,58] V. Thoren,[75] W. H. Tian,[59] Y. Tian,[31,63] Z. F. Tian,[76] I. Uman,[62b] Y. Wan,[55] S. J. Wang,[50] B. Wang,[1] B. L. Wang,[63] Bo Wang,[71,58] D. Y. Wang,[46,h] F. Wang,[72] H. J. Wang,[38,k,l] J. J. Wang,[76] J. P. Wang,[50] K. Wang,[1,58] L. L. Wang,[1] M. Wang,[50] N. Y. Wang,[63] S. Wang,[38,k,l] S. Wang,[12,g] T. Wang,[12,g] T. J. Wang,[43] W. Wang,[59] W. Wang,[72] W. P. Wang,[35,71,o] X. Wang,[46,h] X. F. Wang,[38,k,l] X. J. Wang,[39] X. L. Wang,[12,g] X. N. Wang,[1] Y. Wang,[61] Y. D. Wang,[45] Y. F. Wang,[1,58,63] Y. L. Wang,[19] Y. N. Wang,[45] Y. Q. Wang,[1] Yaqian Wang,[17] Yi Wang,[61] Z. Wang,[1,58] Z. L. Wang,[72] Z. Y. Wang,[1,63] Ziyi Wang,[63] D. H. Wei,[14] F. Weidner,[68] S. P. Wen,[1] Y. R. Wen,[39] U. Wiedner,[3] G. Wilkinson,[69] M. Wolke,[75] L. Wollenberg,[3] C. Wu,[39] J. F. Wu,[1,8] L. H. Wu,[1] L. J. Wu,[1,63] X. Wu,[12,g] X. H. Wu,[34] Y. Wu,[71,58] Y. H. Wu,[55] Y. J. Wu,[31] Z. Wu,[1,58] L. Xia,[71,58] X. M. Xian,[39] B. H. Xiang,[1,63] T. Xiang,[46,h] D. Xiao,[38,k,l] G. Y. Xiao,[42] S. Y. Xiao,[1] Y. L. Xiao,[12,g] Z. J. Xiao,[41] C. Xie,[42] X. H. Xie,[46,h] Y. Xie,[50] Y. G. Xie,[1,58] Y. H. Xie,[6] Z. P. Xie,[71,58] T. Y. Xing,[1,63] C. F. Xu,[1,63] C. J. Xu,[59] G. F. Xu,[1] H. Y. Xu,[66,2,p] M. Xu,[71,58] Q. J. Xu,[16] Q. N. Xu,[30] W. Xu,[1] W. L. Xu,[66] X. P. Xu,[55] Y. C. Xu,[77] Z. P. Xu,[42] Z. S. Xu,[63] F. Yan,[12,g] L. Yan,[12,g] W. B. Yan,[71,58] W. C. Yan,[80] X. Q. Yan,[1] H. J. Yang,[51,f] H. L. Yang,[34] H. X. Yang,[1] T. Yang,[1] Y. Yang,[12,g] Y. F. Yang,[1,63] Y. F. Yang,[43] Y. X. Yang,[1,63] Z. W. Yang,[38,k,l] Z. P. Yao,[50] M. Ye,[1,58] M. H. Ye,[8] J. H. Yin,[1] Z. Y. You,[59] B. X. Yu,[1,58,63] C. X. Yu,[43] G. Yu,[1,63] J. S. Yu,[25,i] T. Yu,[72] X. D. Yu,[46,h] Y. C. Yu,[80] C. Z. Yuan,[1,63] J. Yuan,[34] J. Yuan,[45] L. Yuan,[2] S. C. Yuan,[1,63] Y. Yuan,[1,63] Z. Y. Yuan,[59] C. X. Yue,[39] A. A. Zafar,[73] F. R. Zeng,[50] S. H. Zeng,[72] X. Zeng,[12,g] Y. Zeng,[25,i] Y. J. Zeng,[59] Y. J. Zeng,[1,63] X. Y. Zhai,[34] Y. C. Zhai,[50] Y. H. Zhan,[59] A. Q. Zhang,[1,63] B. L. Zhang,[1,63] B. X. Zhang,[1] D. H. Zhang,[43] G. Y. Zhang,[19] H. Zhang,[71,58] H. Zhang,[80] H. C. Zhang,[1,58,63] H. H. Zhang,[34] H. H. Zhang,[59] H. Q. Zhang,[1,58,63] H. R. Zhang,[71,58] H. Y. Zhang,[1,58] J. Zhang,[80] J. Zhang,[59] J. J. Zhang,[52] J. L. Zhang,[20] J. Q. Zhang,[41] J. S. Zhang,[12,g] J. W. Zhang,[1,58,63] J. X. Zhang,[38,k,l] J. Y. Zhang,[1] J. Z. Zhang,[1,63] Jianyu Zhang,[63] L. M. Zhang,[61] Lei Zhang,[42] P. Zhang,[1,63] Q. Y. Zhang,[34] R. Y. Zhang,[38,k,l] S. H. Zhang,[1,63] Shulei Zhang,[25,i] X. D. Zhang,[45] X. M. Zhang,[1] X. Y. Zhang,[50] Y. Zhang,[72] Y. Zhang,[1] Y. T. Zhang,[80] Y. H. Zhang,[1,58] Y. M. Zhang,[39] Yan Zhang,[71,58] Z. D. Zhang,[1] Z. H. Zhang,[1] Z. L. Zhang,[34] Z. Y. Zhang,[76] Z. Y. Zhang,[43] Z. Z. Zhang,[45] G. Zhao,[1] J. Y. Zhao,[1,63] J. Z. Zhao,[1,58] L. Zhao,[1] Lei Zhao,[71,58] M. G. Zhao,[43] N. Zhao,[78] R. P. Zhao,[63] S. J. Zhao,[80] Y. B. Zhao,[1,58] Y. X. Zhao,[31,63] Z. G. Zhao,[71,58] A. Zhemchugov,[36,b] B. Zheng,[72] B. M. Zheng,[34] J. P. Zheng,[1,58] W. J. Zheng,[1,63] Y. H. Zheng,[63] B. Zhong,[41] X. Zhong,[59] H. Zhou,[50] J. Y. Zhou,[34] L. P. Zhou,[1,63] S. Zhou,[6] X. Zhou,[76] X. K. Zhou,[6] X. R. Zhou,[71,58] X. Y. Zhou,[39] Y. Z. Zhou,[12,g] J. Zhu,[43] K. Zhu,[1]

K. J. Zhu,[1,58,63] K. S. Zhu,[12,g] L. Zhu,[34] L. X. Zhu,[63] S. H. Zhu,[70] S. Q. Zhu,[42] T. J. Zhu,[12,g] W. D. Zhu,[41] Y. C. Zhu,[71,58] Z. A. Zhu,[1,63] J. H. Zou,[1] and J. Zu[71,58]

(BESIII Collaboration)

[1]Institute of High Energy Physics, Beijing 100049, People's Republic of China
[2]Beihang University, Beijing 100191, People's Republic of China
[3]Bochum Ruhr-University, D-44780 Bochum, Germany
[4]Budker Institute of Nuclear Physics SB RAS (BINP), Novosibirsk 630090, Russia
[5]Carnegie Mellon University, Pittsburgh, Pennsylvania 15213, USA
[6]Central China Normal University, Wuhan 430079, People's Republic of China
[7]Central South University, Changsha 410083, People's Republic of China
[8]China Center of Advanced Science and Technology, Beijing 100190, People's Republic of China
[9]China University of Geosciences, Wuhan 430074, People's Republic of China
[10]Chung-Ang University, Seoul 06974, Republic of Korea
[11]COMSATS University Islamabad, Lahore Campus,
Defence Road, Off Raiwind Road, 54000 Lahore, Pakistan
[12]Fudan University, Shanghai 200433, People's Republic of China
[13]GSI Helmholtzcentre for Heavy Ion Research GmbH, D-64291 Darmstadt, Germany
[14]Guangxi Normal University, Guilin 541004, People's Republic of China
[15]Guangxi University, Nanning 530004, People's Republic of China
[16]Hangzhou Normal University, Hangzhou 310036, People's Republic of China
[17]Hebei University, Baoding 071002, People's Republic of China
[18]Helmholtz Institute Mainz, Staudinger Weg 18, D-55099 Mainz, Germany
[19]Henan Normal University, Xinxiang 453007, People's Republic of China
[20]Henan University, Kaifeng 475004, People's Republic of China
[21]Henan University of Science and Technology, Luoyang 471003, People's Republic of China
[22]Henan University of Technology, Zhengzhou 450001, People's Republic of China
[23]Huangshan College, Huangshan 245000, People's Republic of China
[24]Hunan Normal University, Changsha 410081, People's Republic of China
[25]Hunan University, Changsha 410082, People's Republic of China
[26]Indian Institute of Technology Madras, Chennai 600036, India
[27]Indiana University, Bloomington, Indiana 47405, USA
[28a]INFN Laboratori Nazionali di Frascati, I-00044 Frascati, Italy
[28b]INFN Laboratori Nazionali di Frascati, INFN Sezione di Perugia, I-06100 Perugia, Italy
[28c]INFN Laboratori Nazionali di Frascati, University of Perugia, I-06100 Perugia, Italy
[29a]INFN Sezione di Ferrara, I-44122 Ferrara, Italy
[29b]INFN Sezione di Ferrara, University of Ferrara, I-44122 Ferrara, Italy
[30]Inner Mongolia University, Hohhot 010021, People's Republic of China
[31]Institute of Modern Physics, Lanzhou 730000, People's Republic of China
[32]Institute of Physics and Technology, Peace Avenue 54B, Ulaanbaatar 13330, Mongolia
[33]Instituto de Alta Investigación, Universidad de Tarapacá, Casilla 7D, Arica 1000000, Chile
[34]Jilin University, Changchun 130012, People's Republic of China
[35]Johannes Gutenberg University of Mainz, Johann-Joachim-Becher-Weg 45, D-55099 Mainz, Germany
[36]Joint Institute for Nuclear Research, 141980 Dubna, Moscow region, Russia
[37]Justus-Liebig-Universitaet Giessen, II. Physikalisches Institut,
Heinrich-Buff-Ring 16, D-35392 Giessen, Germany
[38]Lanzhou University, Lanzhou 730000, People's Republic of China
[39]Liaoning Normal University, Dalian 116029, People's Republic of China
[40]Liaoning University, Shenyang 110036, People's Republic of China
[41]Nanjing Normal University, Nanjing 210023, People's Republic of China
[42]Nanjing University, Nanjing 210093, People's Republic of China
[43]Nankai University, Tianjin 300071, People's Republic of China
[44]National Centre for Nuclear Research, Warsaw 02-093, Poland
[45]North China Electric Power University, Beijing 102206, People's Republic of China
[46]Peking University, Beijing 100871, People's Republic of China
[47]Qufu Normal University, Qufu 273165, People's Republic of China
[48]Renmin University of China, Beijing 100872, People's Republic of China
[49]Shandong Normal University, Jinan 250014, People's Republic of China

[50]*Shandong University, Jinan 250100, People's Republic of China*
[51]*Shanghai Jiao Tong University, Shanghai 200240, People's Republic of China*
[52]*Shanxi Normal University, Linfen 041004, People's Republic of China*
[53]*Shanxi University, Taiyuan 030006, People's Republic of China*
[54]*Sichuan University, Chengdu 610064, People's Republic of China*
[55]*Soochow University, Suzhou 215006, People's Republic of China*
[56]*South China Normal University, Guangzhou 510006, People's Republic of China*
[57]*Southeast University, Nanjing 211100, People's Republic of China*
[58]*State Key Laboratory of Particle Detection and Electronics,
Beijing 100049, Hefei 230026, People's Republic of China*
[59]*Sun Yat-Sen University, Guangzhou 510275, People's Republic of China*
[60]*Suranaree University of Technology, University Avenue 111, Nakhon Ratchasima 30000, Thailand*
[61]*Tsinghua University, Beijing 100084, People's Republic of China*
[62a]*Turkish Accelerator Center Particle Factory Group, Istinye University, 34010 Istanbul, Turkey*
[62b]*Turkish Accelerator Center Particle Factory Group, Near East University,
Nicosia, North Cyprus 99138, Mersin 10, Turkey*
[63]*University of Chinese Academy of Sciences, Beijing 100049, People's Republic of China*
[64]*University of Groningen, NL-9747 AA Groningen, The Netherlands*
[65]*University of Hawaii, Honolulu, Hawaii 96822, USA*
[66]*University of Jinan, Jinan 250022, People's Republic of China*
[67]*University of Manchester, Oxford Road, Manchester M13 9PL, United Kingdom*
[68]*University of Muenster, Wilhelm-Klemm-Strasse 9, 48149 Muenster, Germany*
[69]*University of Oxford, Keble Road, Oxford OX13RH, United Kingdom*
[70]*University of Science and Technology Liaoning, Anshan 114051, People's Republic of China*
[71]*University of Science and Technology of China, Hefei 230026, People's Republic of China*
[72]*University of South China, Hengyang 421001, People's Republic of China*
[73]*University of the Punjab, Lahore-54590, Pakistan*
[74a]*University of Turin and INFN, University of Turin, I-10125 Turin, Italy*
[74b]*University of Turin and INFN, University of Eastern Piedmont, I-15121 Alessandria, Italy*
[74c]*University of Turin and INFN, INFN, I-10125 Turin, Italy*
[75]*Uppsala University, Box 516, SE-75120 Uppsala, Sweden*
[76]*Wuhan University, Wuhan 430072, People's Republic of China*
[77]*Yantai University, Yantai 264005, People's Republic of China*
[78]*Yunnan University, Kunming 650500, People's Republic of China*
[79]*Zhejiang University, Hangzhou 310027, People's Republic of China*
[80]*Zhengzhou University, Zhengzhou 450001, People's Republic of China*

[a]Deceased
[b]Also at the Moscow Institute of Physics and Technology, Moscow 141700, Russia.
[c]Also at the Novosibirsk State University, Novosibirsk 630090, Russia.
[d]Also at the NRC "Kurchatov Institute", PNPI, 188300 Gatchina, Russia.
[e]Also at Goethe University Frankfurt, 60323 Frankfurt am Main, Germany.
[f]Also at Key Laboratory for Particle Physics, Astrophysics and Cosmology, Ministry of Education; Shanghai Key Laboratory for Particle Physics and Cosmology; Institute of Nuclear and Particle Physics, Shanghai 200240, People's Republic of China.
[g]Also at Key Laboratory of Nuclear Physics and Ion-beam Application (MOE) and Institute of Modern Physics, Fudan University, Shanghai 200443, People's Republic of China.
[h]Also at State Key Laboratory of Nuclear Physics and Technology, Peking University, Beijing 100871, People's Republic of China.
[i]Also at School of Physics and Electronics, Hunan University, Changsha 410082, China.
[j]Also at Guangdong Provincial Key Laboratory of Nuclear Science, Institute of Quantum Matter, South China Normal University, Guangzhou 510006, China.
[k]Also at MOE Frontiers Science Center for Rare Isotopes, Lanzhou University, Lanzhou 730000, People's Republic of China.
[l]Also at Lanzhou Center for Theoretical Physics, Lanzhou University, Lanzhou 730000, People's Republic of China.
[m]Also at the Department of Mathematical Sciences, IBA, Karachi 75270, Pakistan.
[n]Also at Ecole Polytechnique Federale de Lausanne (EPFL), CH-1015 Lausanne, Switzerland.
[o]Also at Helmholtz Institute Mainz, Staudinger Weg 18, D-55099 Mainz, Germany.
[p]Also at School of Physics, Beihang University, Beijing 100191, China.